


RESEARCH

Open Access



Late-stage Anle138b treatment ameliorates tau pathology and metabolic decline in a mouse model of human Alzheimer's disease tau

Matthias Brendel^{1*†} , Maximilian Deussing^{1†}, Tanja Blume^{1,2†}, Lena Kaiser¹, Federico Probst¹, Felix Overhoff¹, Finn Peters², Barbara von Ungern-Sternberg¹, Sergey Ryazanov³, Andrei Leonov^{3,11}, Christian Griesinger^{3,12,13}, Andreas Zwergal⁴, Johannes Levin^{4,5}, Peter Bartenstein^{1,5}, Igor Yakushev^{6,7}, Paul Cumming^{8,9}, Guido Boening¹, Sibylle Ziegler¹, Jochen Herms^{2,5,10}, Armin Giese^{2,11} and Axel Rominger^{1,5,8}

Abstract

Background: Augmenting the brain clearance of toxic oligomers with small molecule modulators constitutes a promising therapeutic concept against tau deposition. However, there has been no test of this concept in animal models of Alzheimer's disease (AD) with initiation at a late disease stage. Thus, we aimed to investigate the effects of interventional late-stage Anle138b treatment, which previously indicated great potential to inhibit oligomer accumulation by binding of pathological aggregates, on the metabolic decline in transgenic mice with established tauopathy in a longitudinal ¹⁸F-fluorodeoxyglucose positron emission tomography (FDG-PET) study.

Methods: Twelve transgenic mice expressing all six human tau isoforms (hTau) and ten controls were imaged by FDG-PET at baseline (14.5 months), followed by randomization into Anle138b treatment and vehicle groups for 3 months. FDG-PET was repeated after treatment for 3 months, and brains were analyzed by tau immunohistochemistry. Longitudinal changes of glucose metabolism were compared between study groups, and the end point tau load was correlated with individual FDG-PET findings.

Results: Tau pathology was significantly ameliorated by late-stage Anle138b treatment when compared to vehicle (frontal cortex – 53%, $p < 0.001$; hippocampus – 59%, $p < 0.005$). FDG-PET revealed a reversal of metabolic decline during Anle138b treatment, whereas the vehicle group showed ongoing deterioration. End point glucose metabolism in the brain of hTau mice had a strong correlation with tau deposition measured by immunohistochemistry ($R = 0.92$, $p < 0.001$).

Conclusion: Late-stage oligomer modulation effectively ameliorated tau pathology in hTau mice and rescued metabolic function. Molecular imaging by FDG-PET can serve for monitoring effects of Anle138b treatment.

Keywords: Tau, Neuronal injury, Late-stage, Anle138b, Small animal PET

* Correspondence: matthias.brendel@med.uni-muenchen.de

†Matthias Brendel, Maximilian Deussing and Tanja Blume contributed equally to this work.

¹Department of Nuclear Medicine, University Hospital, LMU Munich, Marchioninstr.15, 81377 Munich, Germany

Full list of author information is available at the end of the article



Background

Neurofibrillary tangles constitute one of the most characteristic neuropathological findings in Alzheimer's disease (AD), which is the most frequent form of dementia, and tangles likewise occur in certain non-AD dementias known collectively as tauopathies [1]. Several *in vivo* investigations have confirmed a strong link between the presence of hyperphosphorylated tau in the brain, which self-aggregates to paired helical tau filaments and neurofibrillary tangles [2], and future metabolic and cognitive declines in preclinical AD [3–5]. Thus, there is great impetus to develop effective interventions against tau deposition in AD and other neurodegenerative diseases.

Preventive treatment strategies with small molecular weight oligomer modulators of tau, which comprise a suitable pharmacokinetic profile and possess good brain penetration [6], present one promising pharmacological approach to ameliorate tau pathology. This strategy has shown early success in inhibiting tau aggregation *in vitro* and in reducing 4R tau aggregates in P301S mice, which serve as a model for tau-positive frontotemporal dementia [7]. The same treatment also attenuated intracerebral accumulations of α -synuclein in a mouse model of Parkinson's disease [8] and β -amyloid in AD model mice [9]. However, there has hitherto been no direct confirmation of beneficial impacts of oligomer modulator treatment on brain function and tau protein accumulation in transgenic mice expressing human tau protein. Furthermore, the efficacy of late-stage oligomer modulation which emulates a more relevant clinical setting is also unproven.

Molecular brain imaging with ^{18}F -fluorodeoxyglucose positron emission tomography (FDG-PET) is a powerful *in vivo* tool for revealing metabolic deficits in neurodegenerative diseases and has now attained acceptance in the clinical diagnosis of AD [10–12]. Longitudinal FDG-PET is also fit for the preclinical assessment of neuronal injury in a mouse model of tauopathy [13]. Given this background, we aimed to perform an interventional treatment study with the novel aggregation-inhibiting oligomer modulator Anle138b in transgenic mice expressing all six human tau isoforms (hTau), thus constituting a murine model of AD tauopathy [14]. We initiated the treatment at a late disease stage characterized by the presence of tau aggregates, thus emulating a likely clinical scenario. Our main end point for testing the effectiveness of the treatment was serial monitoring of cerebral metabolism by FDG-PET. In addition, we made an end point immunohistochemical assessment of the density of tau pathology after 3 months' treatment with Anle138b as compared to untreated hTau mice. Finally, we undertook a correlational analysis of the relationship between individual tau pathology with longitudinal metabolic decline to FDG-PET.

Materials and methods

Animals and study design

All experiments were carried out in compliance with the German national guidelines for animal protection (TierSchG, Germany) and with approval of the local animal care committee (Regierung von Oberbayern), under supervision by a veterinarian. Experiments, analyses, and reporting were performed in accordance with the ARRIVE guidelines [15]. Animals were housed in a temperature- and humidity-controlled environment with a 12-h light–dark cycle, with free access to food (Ssniff, Soest, Germany) and water. Sample size calculation (G*Power, V3.1.9.2, University of Kiel, Germany) was based on earlier FDG-PET estimates in mice and assuming a type I error $\alpha = 0.05$, a power of 0.8, and a dropout rate of 15% during follow-up. Assuming a relevant treatment effect of 5%, we calculated a group size of six, including one mouse for dropout compensation.

Twelve hTau mice and ten controls (all female) were purchased from Jackson Laboratories (JAX[®]) at 3 months of age and housed in our pathogen-free animal facility until attaining 14.5 months of age. We then undertook baseline FDG-PET imaging and randomized the mice into Anle138b treatment and vehicle treatment groups ($n = 6/5$ each). hTau mice had been designed to express all six isoforms of human tau in similar ratios to that in the diseased human brain, but do not express significant amount of mouse tau [14]. The model was generated by crossing 8c mice that express a tau transgene derived from a human P1-derived artificial chromosome, H1 haplotype [16] together with tau knock-out mice that have a targeted disruption of exon one of the tau gene [17].

The hTau mice that we used are homozygous for *Mapt* <tm1(EGFP)Klt> and heterozygous for *Tg* (NAPT)8cPdav, whereas controls only contain the homozygous *Mapt* <tm1(EGFP)Klt> mutation. Anle138b treatment was administered for 3 months, and follow-up PET imaging was performed in the last week of treatment. After a visual quality check of PET images, we performed transcatheterial perfusion with fixation in 4% paraformaldehyde and brain extraction for immunohistochemical analyses.

Anle138b treatment

We used the oligomer modulator Anle138b ([3-(1,3-benzodioxol-5-yl)-5-(3-bromophenyl)-1H-pyrazole]) [6] as a therapeutic against tau deposition. The compound was formulated in food pellets (Ssniff, Soest, Germany) at a concentration of 2 g/kg pellets [7], which were administered *ad libitum* over a period of 3 months. The food composition was based on regular maintenance diet (16.2 MJ/kg; 9% fat, 24% protein, 67% carbohydrates). Detailed specifications of the Anle138b formulation can be found in supplement #2 of [6]. In brief, (1-(1,3-benzodioxol-5-yl)-3-(3-bromophenyl)propane-1,3-dione), a previously reported pyrazole title

compound [18], was used as a precursor for the chemical synthesis of Anle138b in several steps. Control mice were fed with unmodified food pellets.

PET imaging

PET data acquisition and analyses

All PET procedures followed standardized, established protocols [19]. In brief, mice were anesthetized with isoflurane (1.5%, delivered at 3.5 l/min) and placed in the aperture of the Siemens Inveon DPET [20] as described previously [21]. Mice had been fasted for at least 3 hours prior to tracer administration. Static FDG-PET imaging from 30 to 60 min p.i. was performed after administration of 13.2 ± 2.1 MBq ^{18}F -FDG as previously established [19]. The emission recording was followed by a 15-min transmission scan using rotating ^{57}Co point sources. The image was reconstructed as a single 30-min frame in 4 OSEM3D and 32 MAP 3D iterations, giving a target resolution of 1.0 mm and a zoom factor of 1.0, with scatter-, attenuation-, and decay-correction, resulting in a final voxel dimension of $0.78 \times 0.78 \times 0.80$ mm. Following recovery from anesthesia, mice were returned to their home cages.

PET post-processing

FDG-PET images (30–60 min) were co-registered to an MRI mouse brain atlas [22] by a manual rigid-body transformation (TX_{rigid}) using the PMOD fusion tool (V3.5, PMOD Technologies Ltd.). A reader who was blind to the type of mouse confirmed the initial registration. Then, we applied a reader-independent co-registration by generating treatment group-specific standard FDG-PET templates in the MRI atlas space. Non-linear brain normalization was performed with the PMOD fusion tool for each individual co-registered image to obtain a transformation matrix ($\text{TX}_{\text{BrainNorm}}$) for each mouse brain to the template. The manual (TX_{rigid}) and automatic ($\text{TX}_{\text{BrainNorm}}$) transformations were concatenated and applied to the native space μPET data to guarantee a minimum of interpolation. As the μPET templates had been initially aligned to the atlas, all final fused μPET images had the same spatial orientation and voxel dimensions as the MRI mouse brain atlas, i.e., $0.064 \times 0.064 \times 0.064$ mm.

PET analysis

An oval-shaped frontal cortical volume of interest (VOI; 28 mm^3) and a bilateral circular-shaped hippocampal VOI (11 mm^3) defined in the MRI atlas were placed on the resampled image to calculate the mean radioactivity concentrations in standardized uptake value (SUV) units. Absence of tau pathology in the brainstem of hTau mice has been shown earlier [14], justifying its use as a reference tissue in this mouse model. We calculated the SUV ratios (SUVR_{BST}) as the ratio of the radioactivity concentrations in target and brainstem reference VOIs

of the Mirrione atlas implemented in PMOD [23]. Longitudinal changes were computed for each mouse as the absolute difference of SUVR values between baseline and follow-up scans (ΔSUVR).

Immunohistochemical analyses

After removal from the skull, brains were bisected at the midline and one cerebral hemisphere randomly selected for immunohistochemical analysis after fixation by immersion in 4% paraformaldehyde at 4°C for 24 h. A mean of three representative $50\text{-}\mu\text{m}$ -thick slices per animal was then cut in the sagittal plane between 1.5 and 2.0 mm from the midline using a vibratome (VT 1000 S, Leica, Wetzlar, Germany). Free-floating sections were permeabilized with 2% Triton X-100 overnight and then blocked with I-Block™ Protein-Based Blocking Reagent (Thermo Fischer Scientific). We obtained immunohistochemical labelling of hTau using the CP13 primary antibody (dilution; 1:25, 48 h, RT), which binds specifically to phosphorylated serine 202 (pS202) on tau, followed by incubation with the A-21244 secondary antibody, which contains Alexa Fluor 647 dye (Invitrogen, 1:500) [16, 24]. The unbound dye was removed by three washing steps with PBS, and the slices were then mounted on microscope slides with fluorescent mounting medium (Dako, Germany). Images were acquired with an inverted confocal Laser-Scanning Microscope LSM510=NLO (Zeiss). We imaged the frontal cortex and hippocampus of each slice three-dimensionally in tile scan mode, which allows automatic stitching of an array of fields of view. Tau load (%) in maximum intensity projected image stacks was calculated as the summed area of all tau-positive cells identified using an automated intensity threshold relative to the total inspected area in ImageJ software (Wayne Rasband, (NIH)). Second, we calculated the number of CP13-positive neurons per area (N/mm^2) in the cortex and the hippocampus. The operator was blind to the PET results.

Statistics

Statistics were performed using SPSS (V25, IBM Cooperation) and GraphPad Prism (V5.03). FDG-PET measures of baseline, follow-up assessment, and longitudinal changes, as well as tau burden (%), the number of tau-positive neurons per area and body weight, were compared between the three groups of treated hTau mice, vehicle hTau mice, and non-carrier controls by a one-way ANOVA including Tukey post hoc correction for multiple comparisons. Longitudinal FDG-PET measures in the treatment group were also tested voxel-wise (paired t test) by a statistical parametric mapping approach [25] to allow a region-independent evaluation of metabolic rescue. Body weight was compared by an unpaired Student's t test. For inter-modality correlation analyses, Pearson coefficients of

correlation (R) were calculated between region-specific tau area (%) values and PET read-outs (SUVR, Δ SUVR). A Shapiro–Wilk test was performed to verify normal distribution of sample values (results are provided in Additional file 1). In all tests, a threshold of $p < 0.05$ was considered to be significant for rejection of the null hypothesis.

Results

Late-stage Anle138b treatment reduces tau deposition in hTau mice

First, we investigated if late-stage Anle138b treatment extending over 3 months has the potential to reduce further tau accumulation in mice expressing human AD tau. One mouse of the hTau treatment group died during the baseline PET scan, and one mouse of the hTau vehicle group died between baseline and follow-up, resulting in equally sized groups of five mice for both of the treatment and vehicle groups (carrier and non-carrier). Body weight was initially 18% lower in hTau mice compared to non-carriers at baseline ($p = 0.003$), but there were no significant differences between treatment and vehicle groups at subsequent times (see Additional file 1). CP13 immunohistochemical staining

revealed a clear visual reduction of tau deposition in hTau mice receiving Anle138b treatment when compared to the hTau vehicle group (Fig. 1a–d). Immunohistochemical quantitation indicated a 53% reduction of tau burden after 3 months of Anle138b treatment in the frontal cortex, relative to the burden in hTau vehicle mice (6.1% vs. 13%; $p < 0.001$, Fig. 1e). Similarly, there was 59% less tau burden in the hippocampus of the treated mice (1.9% vs. 4.7; $p < 0.001$, Fig. 1f). There were fewer CP13-positive neurons in the Anle138b treatment group in the frontal cortex (– 33%; $p < 0.001$, Fig. 1g) and the hippocampus (– 14%; $p < 0.001$, Fig. 1g) when compared to the hTau vehicle group.

There was no detectable tau accumulation in non-carrier control mice, irrespective of Anle138b treatment. Table 1 gives a detailed overview of immunohistochemistry findings together with PET findings presented below.

Metabolic decline is rescued by late-stage Anle138b treatment

Next, we aimed to elucidate if late-stage Anle138b treatment has the potential to prevent or rescue metabolic decline. Relative to non-carrier controls, the hTau mice

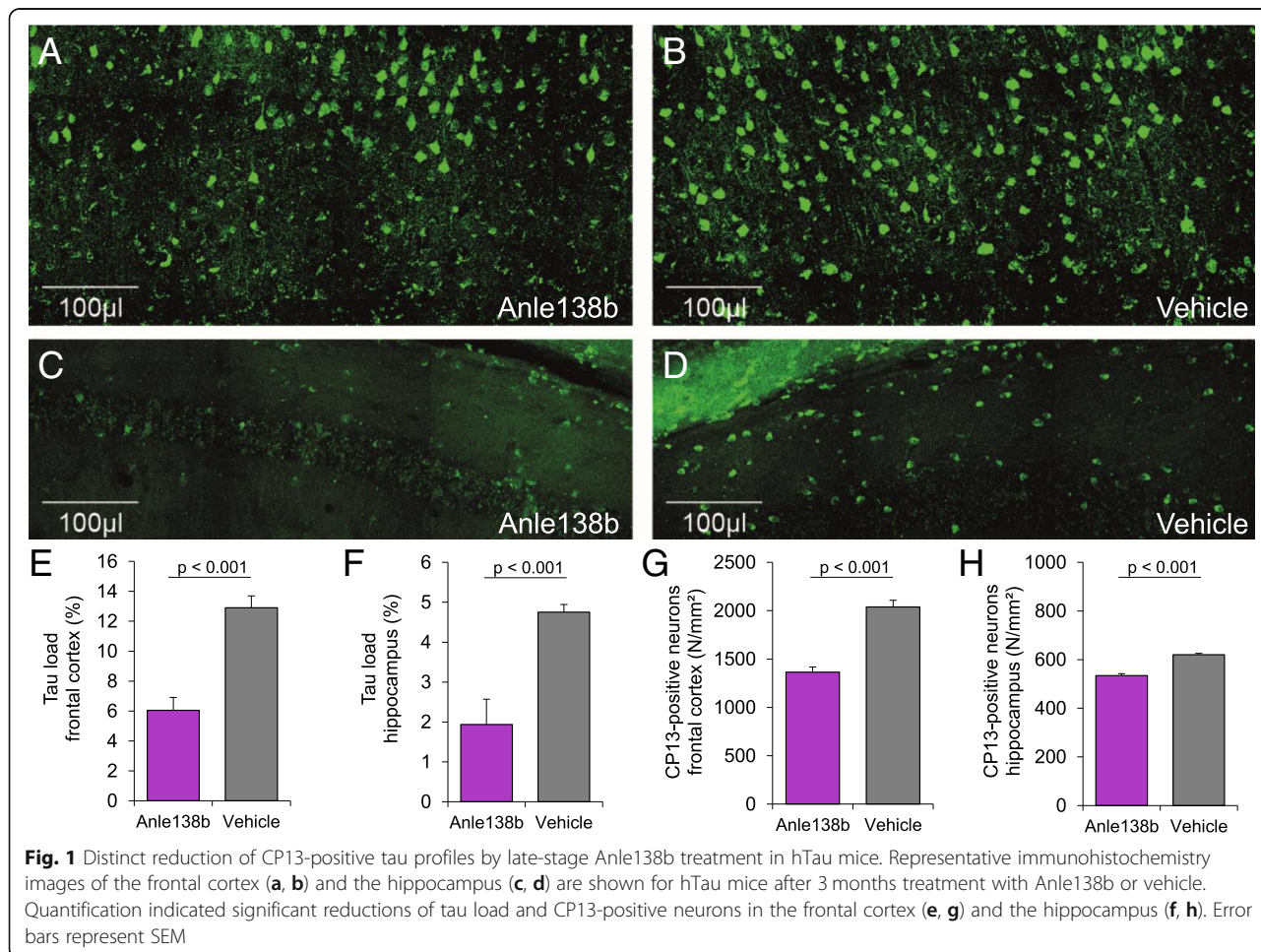


Table 1 Comprehensive overview of end point immunohistochemistry and longitudinal FDG-PET findings in treated and untreated hTau mice

	hTau Anle138b	hTau Vehicle	hTau pooled Baseline	Non-carrier controls (pooled)
Immunohistochemistry Frontal cortex (%-area)	6.1 ± 1.9**	12.9 ± 1.8		0
Immunohistochemistry Frontal cortex (CP13+ neurons, N/mm ²)	1366 ± 116**	2039 ± 153		0
Immunohistochemistry Hippocampus (%-area)	1.9 ± 1.4**	4.8 ± 0.4		0
Immunohistochemistry Hippocampus (CP13+ neurons, N/mm ²)	534 ± 18**	619 ± 13		0
FDG-PET baseline Frontal cortex (SUVR)	0.97 ± 0.02	1.02 ± 0.09	1.00 ± 0.07 [#]	1.10 ± 0.10
FDG-PET follow-up Frontal cortex (SUVR)	1.03 ± 0.05*	0.95 ± 0.03 [#]		1.09 ± 0.06
FDG-PET change Frontal cortex (Δ SUVR)	+ 0.06 ± 0.06*	- 0.07 ± 0.09		+ 0.01 ± 0.05
FDG-PET baseline Hippocampus (SUVR)	0.93 ± 0.03	0.98 ± 0.10	0.96 ± 0.08 [#]	1.06 ± 0.10
FDG-PET follow-up Hippocampus (SUVR)	1.00 ± 0.07	0.93 ± 0.05 ^{##}		1.05 ± 0.07
FDG-PET change Hippocampus (Δ SUVR)	+ 0.06 ± 0.05	- 0.05 ± 0.10		+ 0.00 ± 0.05

Results summary: ** indicates $p < 0.05$ and **** indicates $p < 0.005$ in the direct comparison of hTau treatment and vehicle groups. ^{##} indicates $p < 0.05$ and ^{###} indicates $p < 0.005$ in the comparison of hTau groups (pooled baseline or treatment/vehicle during follow-up) versus non-carrier controls

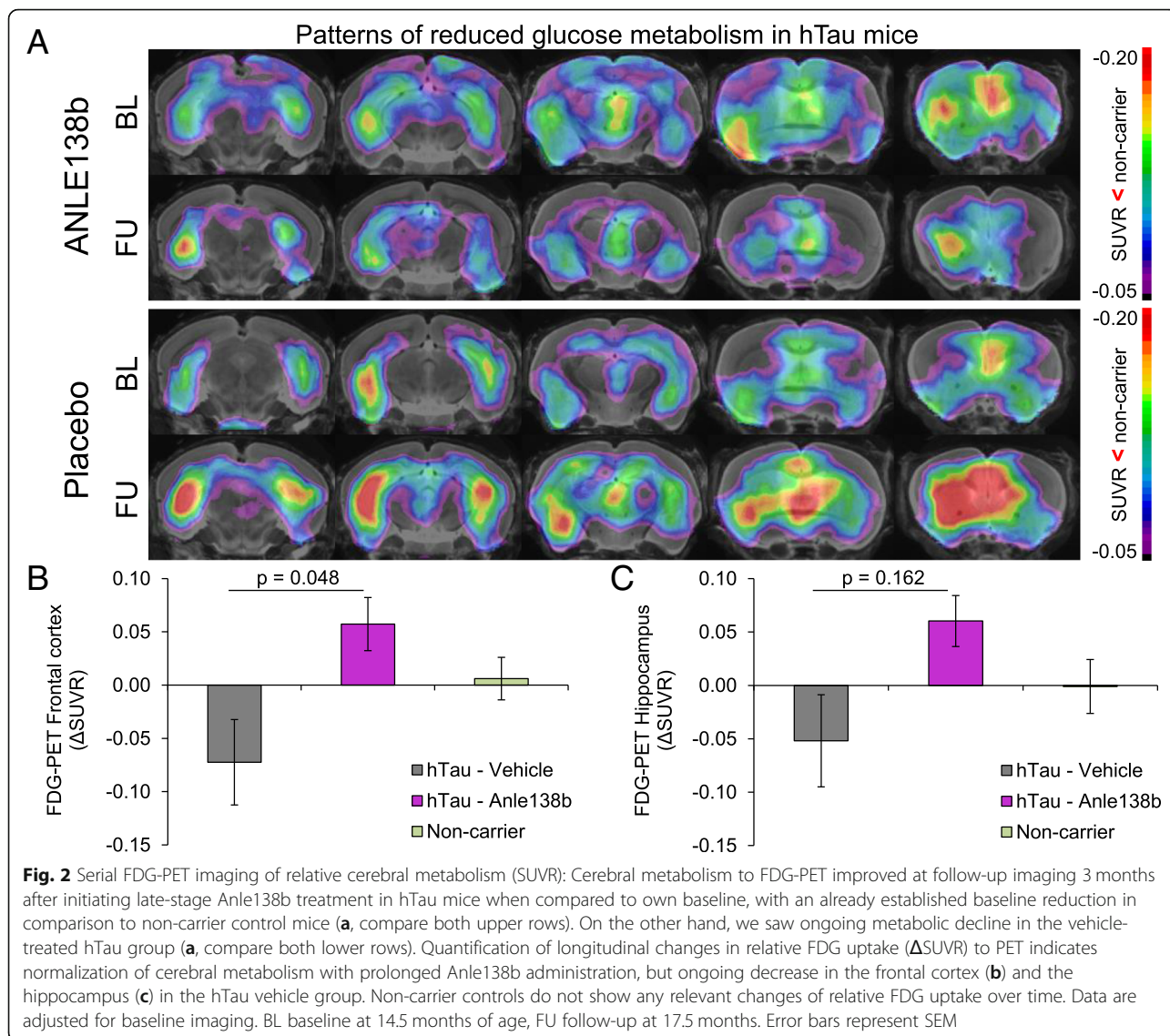
already exhibited moderately reduced relative cerebral FDG uptake at 14.5 months of age (baseline) in the frontal cortex (SUVR - 9%, $p = 0.025$) and in the hippocampus (SUVR - 10%, $p = 0.020$) (Fig. 2). The drug intervention provoked a significant rescue of cerebral metabolism in the frontal cortex of treated hTau mice (Δ SUVR + 6%), whereas the vehicle-treated hTau mice showed further metabolic deterioration (Δ SUVR - 7%, $p = 0.048$; Table 1, Fig. 2). There was likewise a trend towards recovery of metabolism in the hippocampus of treated hTau mice (Δ SUVR + 6% vs - 5%, $p = 0.162$; Table 1). Non-carrier controls did not show any significant changes in cerebral metabolism during the observation period, nor was there any main effect of Anle138b treatment on metabolism (Table 1).

For a region-independent statistical analysis of the potential metabolic rescue, we performed a voxel-wise longitudinal comparison between individual baseline and follow-up FDG SUVR images in the hTau Anle138b treatment group. This analysis revealed significant ($p < 0.01$, $unc\ k > 20$) clusters of increasing relative metabolism in the hippocampus (16,204 voxels, 4.3 mm³, T_{PEAK} 19.2), the somatomotor cortex (18,532 voxels, 4.9 mm³, T_{PEAK} 13.8), the frontal pole (15,268 voxels, 4.0 mm³, T_{PEAK} 14.2), and the thalamus (9594 voxels, 2.5 mm³, T_{PEAK} 8.9) (Fig. 3). Increasing relative cerebral metabolism upon Anle138b treatment was evident to visual inspection of SUVR images in individual hTau mice (Fig. 3).

Vehicle-treated hTau mice showed a strong loss of relative cerebral metabolism in the frontal cortex (- 13%, $p < 0.001$) and the hippocampus (- 12%, $p = 0.007$) at 17.5 months when compared to non-carrier controls. On the other hand, there was only a non-significant trend towards metabolic decline in the same contrast for the hTau Anle138b treatment group (- 6%, $p = 0.101$, hippocampus - 5%, $p = 0.369$).

Tau pathology and metabolic decline are closely associated in hTau mice

Finally, we asked if our observations of attenuated metabolic decline in the treated mice are indeed attributable to reduced tau deposition. To test this, we performed a correlation analysis between read-outs of FDG-PET SUVR and tau burden in both of our target areas. Importantly, end point tau burden as assessed by immunohistochemistry in the frontal cortex had an extraordinarily strong negative correlation with the corresponding end point FDG-PET signal within the complete group of hTau mice ($R = -0.92$, $p < 0.001$, Fig. 4a). There were also negative correlations when considering the hTau vehicle ($R = -0.90$, $p = 0.036$) or the hTau treatment group ($R = -0.90$, $p = 0.035$) separately, meaning that metabolic function deteriorated in concert with tau deposition. Furthermore, we also observed a negative association between the longitudinal change of relative FDG uptake and the end point tau burden ($R = -0.77$, $p = 0.010$, Fig. 4c), which gives additional evidence for the interrelationship of the two



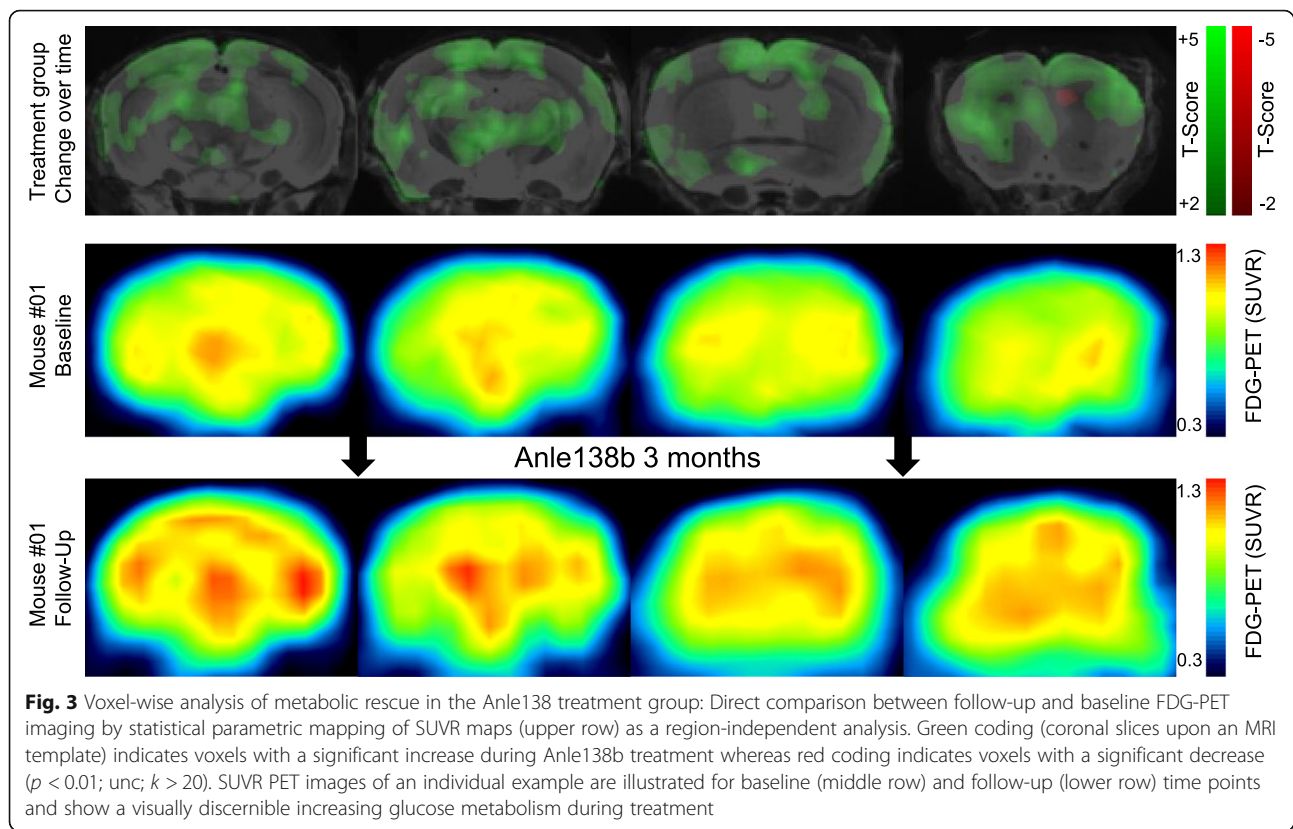
biomarkers. End point FDG-PET ($R = 0.81, p = 0.004$) and longitudinal changes of relative FDG uptake ($R = 0.69, p = 0.026$) were also negatively correlated with the number of CP13-positive neurons in the neocortex, when considering all hTau mice. Findings in the hippocampus mirrored the results for the frontal cortex, but with lesser correlations (Fig. 4b, d, f, h).

Discussion

We present the first study documenting an in vivo proof of rescued metabolic function to longitudinal FDG-PET in mice expressing human tau after receiving a late-stage oligomer modulator treatment. Furthermore, our end point immunohistochemical data give clear evidence that tau deposition was reduced in treated mice, in proportion to the rescue from metabolic decline. Thus, Anle138b holds promise to improve even established decline of glucose

consumption by promoting reduction of CP13-positive hyperphosphorylated tau aggregates and less neurons with CP13-positive tau accumulation, which may bode well for future translational interventional studies of human AD.

Anle138b is already of proven efficacy in lowering tau deposition in the 4R mouse PS19 tauopathy model and caused an increased survival rate in these mice, when administered in chow from weaning to terminal disease [7]. The aim of the current study was to prove the drug's performance when initiated rather as a late-stage treatment of tauopathy in an AD-like mouse model characterized by paired helical 3R/4R tau and slow disease progression resembling aspects of the human disease [14]. Late-stage initiation seems more relevant to translation into clinical testing, as patients will likely have an already established tau load at the time of diagnosis. Tau deposition in the neocortex and the hippocampus of our



hTau mice was more than halved by Anle138b treatment ($-53\%/-59\%$) in comparison to vehicle fed mice, an effect consistent with earlier observations in similarly treated PS19 mice. Thus, we observed the anticipated beneficial effect of Anle138b oligomer modulator treatment on AD-like tau pathology also for this paradigm of late-stage treatment initiation. Nevertheless, the regional distribution of pathology and neuronal dysfunction in these hTau mice (neocortical and hippocampal) closely reflects the topology of human AD tau deposition. In contrast, PS19 tauopathy mice primarily exhibit pathology in the hindbrain, which leads to early death due to motor impairment and respiratory failure [26]. The regional pattern of tau deposition in our hTau mice also matched the pattern of baseline FDG-PET deficits, which clearly indicated reduced relative FDG uptake in the hippocampus and frontal cortex, already evident at the baseline examination at 14.5 months (Fig. 2a).

The feasibility of detection and monitoring loss of cerebral metabolism by serial FDG-PET in tau model mice was also well-supported by a recent study [13] showing decreased FDG-PET uptake in transgenic tau-VWL mice already at 11 months, which further progressed to 19 months of age. Therefore, we aimed in the present study to untangle a crucial question: does an intervention against the primary pathology caused by the transgene in the mouse model rescue or rectify the

AD-like metabolic decline, where reduced FDG uptake is a surrogate for progressive failure of neuronal function? This is an important consideration in light of several failed AD vaccination trials targeting β -amyloid pathology [27, 28], which succeeded in clearing the therapy target from the brain but failed to improve cognition as their primary end point. The association between cognitive performance and neuronal dysfunction/injury is modulated by diverse factors and moderated by cognitive reserve [29]. In this regard, biomarkers of neuronal injury are important read-outs, as they resemble the desired functional therapy outcome. FDG-PET, which traces cerebral glucose consumption, is widely used for the assessment of neuronal injury and diagnosis of neurodegenerative diseases [30] and has served for therapy monitoring in AD drug trials [31]. Most diagnostic schemes of AD employed by international working groups now include biomarkers of neuronal injury together with $A\beta$ and tau protein deposition [10–12]. Pre-clinical FDG-PET imaging has the clear advantage of delivering robust values even in individual mice and allows adjustment for varying baseline measures [19].

Our findings of attenuated metabolic decline with Anle138b treatment initiated at a late disease stage are compelling as they show inhibition or even dispersal of established tau aggregates, along with rebound of the previously impaired cerebral metabolism (Fig. 3). This means

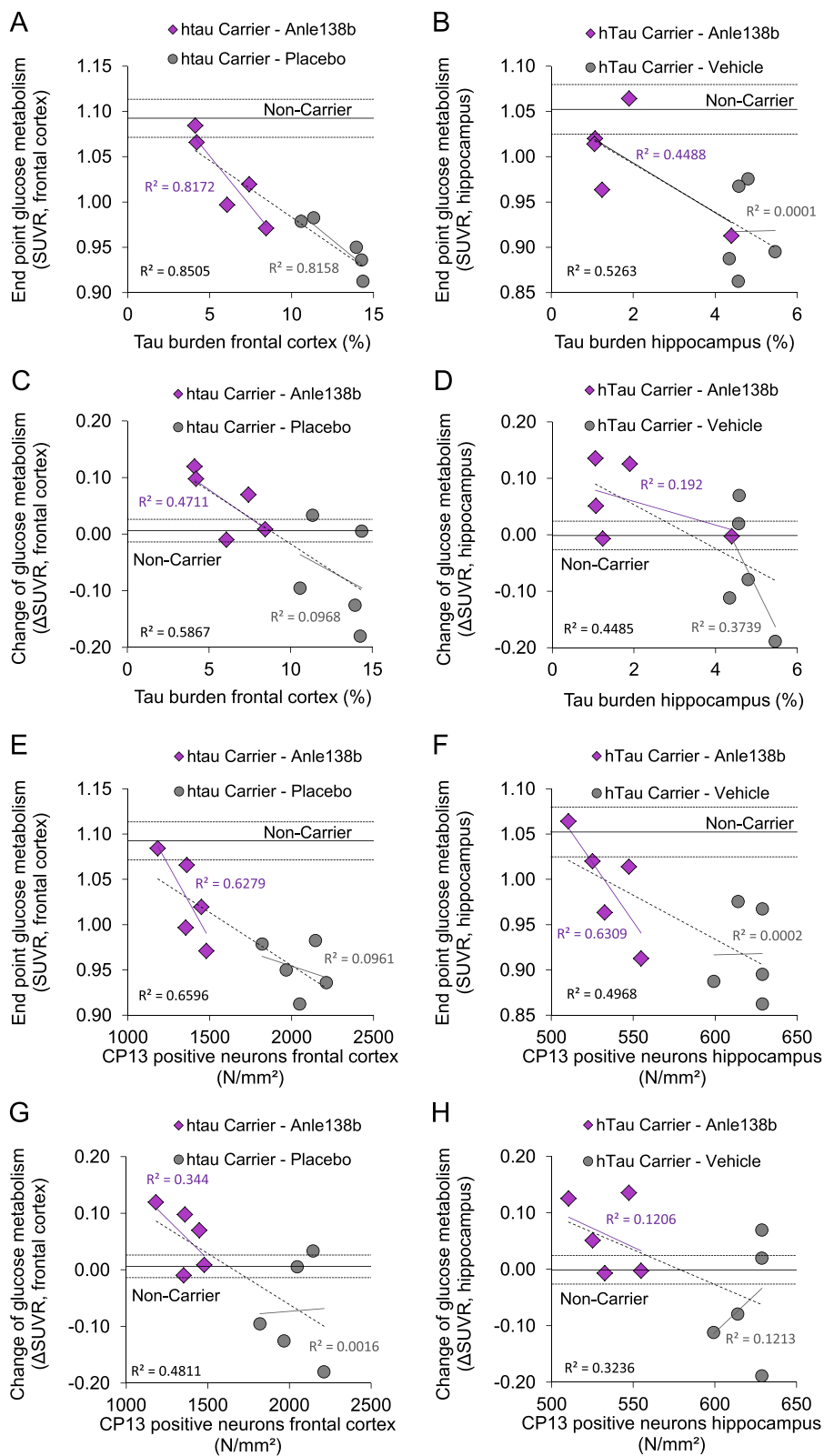


Fig. 4 (See legend on next page.)

(See figure on previous page.)

Fig. 4 Correlation analysis of metabolic function and end point tau assessments: The end point tau burden and the number of CP13-positive neurons per unit area in the frontal cortex had strong negative correlations with end point findings (**a, e**) and longitudinal changes (**c, g**) of normalized FDG uptake in hTau mice. Corresponding plots for the hippocampus indicate the same negative correlation between tau burden and region-specific relative glucose metabolism (**b, d, f, h**). Purple trendlines show the linear association within the hTau treatment group, whereas the gray trendline provides the linear association for the hTau vehicle group. The dashed black line illustrates the linear association of combined hTau mice. Associated R^2 values are indicated in the same color. Solid and dotted lines of non-carrier controls show mean \pm SEM

that the loss of brain energy metabolism arising from tau pathology is recoverable to some degree after rectifying the tauopathy. In clinical translation, sporadic AD patients will likely initiate treatment at an established disease stage, similar to our late-stage treatment paradigm as tau pathology is already established in mild cognitive impairment. Thus, the ability to halt or even improve metabolic function at late disease stages is an invaluable property for drugs targeting tau pathology, as in the present Anle138b study of tauopathy mice. This stands in contrast to pre-clinical results with γ -secretase-modulation and β -secretase-inhibition, which clearly lost their effectiveness once amyloid β -amyloid pathology was established [32, 33]. Nevertheless, potential differences between the mouse model and the situation in human AD need to be considered for interpretation of the results as the investigated mouse model exhibits only tau pathology, without β -amyloid accumulation. Thus, it might be more difficult to halt or improve metabolic decline by late-stage AD treatment in humans, given that the onset of tau pathology is likely triggered by initial amyloid accumulation [34].

Importantly, we find a clear negative association between the end point tau burden in the brain of hTau mice and the extent of impaired cerebral metabolism to longitudinal FDG-PET (Fig. 4). These data support a physiological linkage between AD-like tau pathology and metabolic decline. The rescue of metabolic decline after initiating oligomer treatment strengthens further this mechanistic concept. Previous human studies using PET and assays of tau in cerebrospinal fluid [3, 4] also suggested an association between tau pathology and metabolic decline, despite lacking the histopathological gold standard assessments. Thus, to our knowledge, we provide the first demonstration of a direct correlation between metabolic decline and AD tau deposition, as assessed by gold standard immunohistochemistry. Interestingly, the neocortical FDG uptake of the two hTau mice with lowest tau pathology after Anle138b treatment attained the range of non-carrier control mice (Fig. 4a). Future studies with large sample sizes might be able to define a threshold of tau pathology manifesting in neuronal dysfunction. Keeping in mind earlier investigations showing a direct linkage between metabolic changes and tau phosphorylation [35], we note as a limitation

that we cannot entirely rule out a direct influence of the observed metabolic changes in FDG-PET on the rate of tau phosphorylation. Subsequently, alterations of pS202 phosphorylation could have had an impact on the intensity of the CP13 immunohistochemical staining, which was however qualitatively similar in the CP13-positive neuronal population. However, we also observed a clear treatment effect on the number of CP13-positive neurons, and we do not deem it likely that some non-specific treatment effect on global metabolic changes would completely ameliorate the CP13 signal of single neurons.

Future preclinical studies of Anle138b treatment might properly include tau PET to allow longitudinal monitoring of tau pathology in hTau mice. We previously established ^{18}F -THK5117 PET in different tau mouse models [25], but were unable to see specific PET signal in untreated hTau mice even at 17.5 months of age (data not shown). This failure probably relates to the rather high detection threshold of first-generation tau PET ligands ($\sim 10\%$) and the very low magnitude of advanced forms of tau (discussed below) in hTau mice, which represent the target of arylquinoline tau ligands. Nonetheless, the current development of second-generation tau PET ligands [36] with reduced off-target binding and higher signal to noise ratio will potentially solve this technical issue. Recent establishment of the SV2A PET assay of synaptic density [37] might further enhance future study designs by affording a more direct index of synaptic integrity compared to FDG-PET. Although the FDG-PET signal is a valid surrogate for synaptic activity [38], it can also be altered by factors such as neuroinflammation or blood glucose levels. The current results call for inclusion of spatial learning tasks in future Anle138b studies with larger sample sizes.

Among the limitations of our study, we note that for technical reasons biochemical analyses of tau concentration were unavailable. Furthermore, tau pathology was only assessed by a single immunohistochemical measure targeting pS202, since Gallyas staining did not give a specific tau signal in this material (data not shown). The apparently negative Gallyas staining in untreated hTau mice at 17.5 months of age suggests only that there was an unexpectedly low degree of advanced tau aggregate forms in these mice. We speculate that our housing of the transgenic mice in a pathogen-free environment for more

than 10 months before imaging might have had an impact on the severity of pathology expressed in this model.

Conclusion

Late-stage initiation of oligomer modulation by Anle138b effectively ameliorated AD-like tau pathology in hTau mice while rescuing the declining cerebral metabolism to FDG-PET. Late-stage treatments with efficacy despite established brain pathology at the initiation of treatment are highly desirable for AD, and the present preclinical results are encouraging for the use of agents like Anle138b.

Additional file

Additional file 1: Results of normal distribution testing and longitudinal measures of body weight. (DOCX 16 kb)

Abbreviations

18F: Flour-isotope with mass number 18; 3R: Three repeat; 4R: Four repeat; 57Co: Cobalt-isotope with mass number 57; AD: Alzheimer's disease; BL: Baseline; BST: Brainstem; FDG: Fluorodesoxyglucose; FU: Follow-up; k: Number of voxels; Mapt: Microtubule-associated protein tau; MRI: Magnetic resonance imaging; OSEM: Three-dimensional ordered-subset-expectation-maximum; p.i.: Post injection; PBS: Phosphate-buffered saline; PET: Positron emission tomography; *R*: Pearson coefficients of correlation; SEM: Standard error of the mean; SUV: Standardized uptake value; SUV_R: Standardized uptake value ratio; Tg: Transgene; TX: Transformation; unc: Uncorrected; VOI: Volume of interest; vs: Versus; Δ%: Percentage change; μPET: Small animal positron emission tomography

Acknowledgements

We thank Karin Bormann-Giglmaier and Rosel Oos for the excellent technical assistance. CP13 antibody was kindly provided by Peter Davies (Dominick P. Purpura Department of Neuroscience and Department of Pathology, Albert Einstein College of Medicine, Bronx, New York 10461).

Authors' contributions

MB, MD, FP, and FO performed the PET experiments and analyses. TB and FP performed immunohistochemistry experiments and analyses. MB, MD, and TB analyzed and quantified the data together with the support from LK, GB, and SZ. BU-S supervised the study as a veterinarian. SR, AL, and CG invented Anle138b. AZ and JL designed the trial and adjusted the mouse model to match clinical prospects. PB, IY, and PC interpreted the PET data. MB, JH, AG, and AR contributed to the conception and design of the study. MB, MD, TB, and PC wrote the manuscript. All authors participated in the generation of the original data, added important intellectual content to the manuscript, and provided critical assessment of the current manuscript. All authors read and approved the final manuscript.

Funding

The study was financially supported by the SyNergy Cluster and the European Union's Seventh Framework Programme FP7/2013-2017/ under MINDView grant agreement no [603002] and the Max Planck Society and the Deutsche Forschungsgemeinschaft (DFG, German Research Foundation) under Germany's Excellence Strategy-EXC 2067/1-390729940.

Availability of data and materials

The datasets used and/or analyzed during the current study are available from the corresponding author upon reasonable request.

Ethics approval and consent to participate

All experiments were carried out in compliance with the National Guidelines for Animal Protection, Germany, with the approval of the regional Animal Care Committee of the Government of Oberbayern (Regierung Oberbayern) and were overseen by a veterinarian. Animal experiments were conducted in

accordance with the guidelines EU Directive 2010/63/EU and ARRIVE for animal experiments.

Consent for publication

Not applicable.

Competing interests

SR, AL, AG, and CG are inventors in a patent application related to the compound use in this study. AG and CG are co-founders of MODAG. AL is partly employed by MODAG. All other authors declare that they have no competing interests.

Author details

¹Department of Nuclear Medicine, University Hospital, LMU Munich, Marchioninstr.15, 81377 Munich, Germany. ²German Center for Neurodegenerative Diseases (DZNE), Munich, Germany. ³Max Planck Institute for Biophysical Chemistry, Göttingen, Germany. ⁴Department of Neurology, University Hospital, LMU Munich, Munich, Germany. ⁵Munich Cluster for Systems Neurology (SyNergy), Munich, Germany. ⁶Neuroimaging Center (TUM-NIC), Technische Universität München, Munich, Germany. ⁷Department of Nuclear Medicine, Technical University of Munich, Munich, Germany. ⁸Department of Nuclear Medicine, Inselspital Bern, Bern, Switzerland. ⁹School of Psychology and Counselling and IHBI, Queensland University of Technology, Brisbane, Australia. ¹⁰Center for Neuropathology and Prion Research, Ludwig-Maximilians-Universität, Feodor Lynen-Str. 23, 81377 Munich, Germany. ¹¹MODAG GmbH, 55324 Wendelsheim, Germany. ¹²DFG Research Centre Nanoscale Microscopy and Molecular Physiology of the Brain, 37070 Göttingen, Germany. ¹³Cluster of Excellence "Multiscale Bioimaging: from Molecular Machines to Networks of Excitable Cells" (MBExC), University of Göttingen, Göttingen, Germany.

Received: 28 March 2019 Accepted: 22 July 2019

Published online: 01 August 2019

References

- Duyckaerts C, Delatour B, Potier MC. Classification and basic pathology of Alzheimer disease. *Acta Neuropathol.* 2009;118:5–36.
- Cowan CM, Mudher A. Are tau aggregates toxic or protective in tauopathies? *Front Neurol.* 2013;4:114.
- Pascoal TA, Mathotaarachchi S, Mohades S, et al. Amyloid-beta and hyperphosphorylated tau synergy drives metabolic decline in preclinical Alzheimer's disease. *Mol Psychiatry.* 2017;22:306–11.
- Chiotis K, Saint-Aubert L, Rodriguez-Vieitez E, et al. Longitudinal changes of tau PET imaging in relation to hypometabolism in prodromal and Alzheimer's disease dementia. *Mol Psychiatry.* 2018;23(7):1666–73.
- Pascoal TA, Mathotaarachchi S, Shin M, et al. Amyloid and tau signatures of brain metabolic decline in preclinical Alzheimer's disease. *Eur J Nucl Med Mol Imaging.* 2018;45:1021–30.
- Wagner J, Ryazanov S, Leonov A, et al. Anle138b: a novel oligomer modulator for disease-modifying therapy of neurodegenerative diseases such as prion and Parkinson's disease. *Acta Neuropathol.* 2013;125:795–813.
- Wagner J, Krauss S, Shi S, et al. Reducing tau aggregates with anle138b delays disease progression in a mouse model of tauopathies. *Acta Neuropathol.* 2015;130:619–31.
- Levin J, Schmidt F, Boehm C, et al. The oligomer modulator anle138b inhibits disease progression in a Parkinson mouse model even with treatment started after disease onset. *Acta Neuropathol.* 2014;127:779–80.
- Martinez Hernandez A, Urbanke H, Gillman AL, et al. The diphenylpyrazole compound anle138b blocks Abeta channels and rescues disease phenotypes in a mouse model for amyloid pathology. *EMBO Mol Med.* 2018;10:32–47.
- Dubois B, Feldman HH, Jacova C, et al. Advancing research diagnostic criteria for Alzheimer's disease: the IWG-2 criteria. *Lancet Neurol.* 2014;13:614–29.
- Jack CR Jr, Bennett DA, Blennow K, et al. A/T/N: an unbiased descriptive classification scheme for Alzheimer disease biomarkers. *Neurology.* 2016;87:539–47.
- McKhann GM, Knopman DS, Chertkow H, et al. The diagnosis of dementia due to Alzheimer's disease: recommendations from the National Institute on Aging-Alzheimer's Association workgroups on diagnostic guidelines for Alzheimer's disease. *Alzheimers Dement.* 2011;7:263–9.

13. de Cristobal J, Garcia-Garcia L, Delgado M, Perez M, Pozo MA, Medina M. Longitudinal assessment of a transgenic animal model of tauopathy by FDG-PET imaging. *J Alzheimers Dis.* 2014;40(Suppl 1):S79–89.
14. Andorfer C, Kress Y, Espinoza M, et al. Hyperphosphorylation and aggregation of tau in mice expressing normal human tau isoforms. *J Neurochem.* 2003;86:582–90.
15. Kilkenny C, Browne WJ, Cuthill IC, Emerson M, Altman DG. Improving bioscience research reporting: the ARRIVE guidelines for reporting animal research. *PLoS Biol.* 2010;8:e1000412.
16. Duff K, Knight H, Refolo LM, et al. Characterization of pathology in transgenic mice over-expressing human genomic and cDNA tau transgenes. *Neurobiol Dis.* 2000;7:87–98.
17. Tucker KL, Meyer M, Barde YA. Neurotrophins are required for nerve growth during development. *Nat Neurosci.* 2001;4:29–37.
18. Chauhan SS, Sharma A, Saingar S, Joshi Y. Solid phase synthesis of novel pyrazole derivatives from diaryl 1, 3-diketones under microwave irradiation. *ChemInform.* 2006;37:no-no.
19. Brendel M, Probst F, Jaworska A, et al. Glial activation and glucose metabolism in a transgenic amyloid mouse model: a triple-tracer PET study. *J Nucl Med.* 2016; 57:954–60.
20. Visser EP, Disselhorst JA, Brom M, et al. Spatial resolution and sensitivity of the Inveon small-animal PET scanner. *J Nucl Med.* 2009;50:139–47.
21. Rominger A, Mille E, Zhang S, et al. Validation of the octomouse for simultaneous 18F-fallypride small-animal PET recordings from 8 mice. *J Nucl Med.* 2010;51:1576–83.
22. Dorr A, Sled JG, Kabani N. Three-dimensional cerebral vasculature of the CBA mouse brain: a magnetic resonance imaging and micro computed tomography study. *Neuroimage.* 2007;35:1409–23.
23. Ma Y, Hof PR, Grant SC, et al. A three-dimensional digital atlas database of the adult C57BL/6J mouse brain by magnetic resonance microscopy. *Neuroscience.* 2005;135:1203–15.
24. Polydoro M, Acker CM, Duff K, Castillo PE, Davies P. Age-dependent impairment of cognitive and synaptic function in the htau mouse model of tau pathology. *J Neurosci.* 2009;29:10741–9.
25. Brendel M, Jaworska A, Probst F, et al. Small-animal PET imaging of tau pathology with 18F-THK5117 in 2 transgenic mouse models. *J Nucl Med.* 2016;57:792–8.
26. Yoshiyama Y, Higuchi M, Zhang B, et al. Synapse loss and microglial activation precede tangles in a P301S tauopathy mouse model. *Neuron.* 2007;53:337–51.
27. The Lancet N. Solanezumab: too late in mild Alzheimer's disease? *Lancet Neurol.* 2017;16:97.
28. Vandenberghe R, Rinne JO, Boada M, et al. Bapineuzumab for mild to moderate Alzheimer's disease in two global, randomized, phase 3 trials. *Alzheimers Res Ther.* 2016;8:18.
29. Ewers M, Insel PS, Stern Y, Weiner MW. Alzheimer's disease neuroimaging I. Cognitive reserve associated with FDG-PET in preclinical Alzheimer disease. *Neurology.* 2013;80:1194–201.
30. Laforce R Jr, Soucy JP, Sellami L, et al. Molecular imaging in dementia: past, present, and future. *Alzheimers Dement.* 2018;14(11):1522–52.
31. Dodel R, Rominger A, Bartenstein P, et al. Intravenous immunoglobulin for treatment of mild-to-moderate Alzheimer's disease: a phase 2, randomised, double-blind, placebo-controlled, dose-finding trial. *Lancet Neurol.* 2013;12:233–43.
32. Brendel M, Jaworska A, Herms J, et al. Amyloid-PET predicts inhibition of de novo plaque formation upon chronic gamma-secretase modulator treatment. *Mol Psychiatry.* 2015;20:1179–87.
33. Brendel M, Jaworska A, Overhoff F, et al. Efficacy of chronic BACE1 inhibition in PS2APP mice depends on the regional A beta deposition rate and plaque burden at treatment initiation. *THERANOSTICS.* 2018;8:4957–68.
34. Pontecorvo MJ, Devous MD Sr, Navitsky M, et al. Relationships between flortaucipir PET tau binding and amyloid burden, clinical diagnosis, age and cognition. *Brain.* 2017;140:748–63.
35. Planel E, Miyasaka T, Launey T, et al. Alterations in glucose metabolism induce hypothermia leading to tau hyperphosphorylation through differential inhibition of kinase and phosphatase activities: implications for Alzheimer's disease. *J Neurosci.* 2004;24:2401–11.
36. Betthauser TJ, Cody KA, Zammit MD, et al. In vivo characterization and quantification of neurofibrillary tau PET radioligand [(18F)MK-6240] in humans from Alzheimer's disease dementia to young controls. *J Nucl Med.* 2019;60(1):93–9.
37. Finnema SJ, Nabulsi NB, Mercier J, et al. Kinetic evaluation and test-retest reproducibility of [(11)C]UCB-J, a novel radioligand for positron emission tomography imaging of synaptic vesicle glycoprotein 2A in humans. *J Cereb Blood Flow Metab.* 2017;271678X17724947.
38. Sokoloff L, Reivich M, Kennedy C, et al. The [14C] deoxyglucose method for the measurement of local cerebral glucose utilization: theory, procedure, and normal values in the conscious and anesthetized albino rat. *J Neurochem.* 1977;28:897–916.

Publisher's Note

Springer Nature remains neutral with regard to jurisdictional claims in published maps and institutional affiliations.

Ready to submit your research? Choose BMC and benefit from:

- fast, convenient online submission
- thorough peer review by experienced researchers in your field
- rapid publication on acceptance
- support for research data, including large and complex data types
- gold Open Access which fosters wider collaboration and increased citations
- maximum visibility for your research: over 100M website views per year

At BMC, research is always in progress.

Learn more [biomedcentral.com/submissions](https://www.biomedcentral.com/submissions)

